Journal of Power Sources 195 (2010) 5032–5038

Contents lists available at ScienceDirect

Journal of Power Sources

journal homepage: www.elsevier.com/locate/jpowsour

Al-doped spinel $LiAl_{0.1}Mn_{1.9}O_4$ with improved high-rate cyclability in aqueous electrolyte

Anbao Yuan*, Lei Tian, Wanmei Xu, Yuqin Wang

Department of Chemistry, College of Sciences, Shanghai University, Shanghai 200444, PR China

ARTICLE INFO

Article history:
Received 20 November 2009
Received in revised form 27 January 2010
Accepted 28 January 2010
Available online 4 February 2010

Keywords:
Spinel lithium manganese oxide
Aluminum doping
Solid grinding reaction
Calcination
Cyclability
Aqueous electrolyte

ABSTRACT

To improve the cyclability of spinel $LiMn_2O_4$ in aqueous electrolyte, Al-doped $LiAl_xMn_{2-x}O_4$ ($x = 0.05$, 0.1, 0.15) materials are prepared using a room-temperature solid-state grinding reaction followed by calcination at different temperatures for different durations, respectively. Their phase structures and morphologies are characterized by X-ray diffraction (XRD) and transmission electron microscopy (TEM) techniques. Electrochemical performances of the materials are investigated by cyclic voltammetry and galvanostatic charge/discharge methods. XRD results reveal that the crystallinity of the $LiAl_{0.1}Mn_{1.9}O_4$ increases with increasing calcination temperature and calcination time. However, when the calcination temperature is increased to 800 °C, a small amount of Mn_3O_4 impurity phase is detected in the product calcined for 12 h, due to the decomposition of $LiAl_{0.1}Mn_{1.9}O_4$, while the product calcined for a shorter time of 3 or 6 h is found to be $LiAl_{0.1}Mn_{1.9}O_4$ single phase. TEM results confirm that the grain size of the materials increases with increasing calcination temperature. Electrochemical experiments demonstrate that the charge/discharge cyclability of the $LiAl_{0.1}Mn_{1.9}O_4$ increases with increase in calcination temperature and calcination time. Compared with the pristine $LiMn_2O_4$, the Al-doped $LiAl_xMn_{1-x}O_4$ show the obviously improved cyclability, especially for the $LiAl_{0.1}Mn_{1.9}O_4$ calcined at an elevated temperature for 12 h.

1. Introduction

Spinel lithium manganese oxide ($LiMn_2O_4$) with the merits of abundant manganese resources, low cost and low toxicity, is a most promising candidate material for nonaqueous lithium ion batteries [1,2]. However, its cyclic stability is poor in nonaqueous electrolytes, especially at a higher temperature above 55 °C. Although the exact reason for this phenomenon has not been fully understood yet, the possible reasons responsible for the quick fading of capacity are generally believed to originate from three aspects [3,4]: (i) Jahn–Teller distortion of the cubic spinel structure of $LiMn_2O_4$ during discharging with increase in Mn^{3+} in the structure; (ii) gradually dissolution of Mn^{3+} to electrolyte via disproportionation reaction; (iii) decomposition of organic solvent at higher potentials. It has well been demonstrated that the cyclic stability of $LiMn_2O_4$ could be improved by bulk-phase chemically doping [3–11] or surface coating [12–15]. Several elements were found to be effective for doping, such as Al [3–5], Cr [6–8] and Ni [9–11] etc.

On the other hand, in 1994, Dahn and co-workers [16] first reported an aqueous lithium ion battery based on $LiMn_2O_4$ positive electrode, VO_2(B) negative electrode and 5 M $LiNO_3$ aqueous electrolyte. Thereafter, aqueous lithium ion batteries attracted the interests of researchers gradually. There have been some electrochemical studies of $LiMn_2O_4$ in aqueous electrolytes [17–29], but few studies are about doped $LiMn_2O_4$ [20,24]. One paper investigated the structure variation of the Al-doped $LiAl_{0.15}Mn_{1.85}O_4$ during charge and discharge in a $LiNO_3$ solution by in situ X-ray diffraction (XRD) method [20]. Another paper studied the cyclic voltammetric behavior of the Cr-doped $LiCr_{0.15}Mn_{1.85}O_4$ electrode in a $LiNO_3$ solution in comparison with that in nonaqueous electrolyte [24]. However, the two studies did not report constant-current charge/discharge performance and cyclic stability of the doped $LiMn_2O_4$ electrodes in aqueous electrolytes.

Recently, we reported a comparative study on electrochemical performances of a nanostructured pristine (undoped) $LiMn_2O_4$ in 2 M Li_2SO_4 in comparison with those in different concentrations of $LiNO_3$ aqueous electrolytes [29]. The $LiMn_2O_4$ material was prepared using a room-temperature solid-phase grinding reaction starting with lithium acetate ($LiOAc{\cdot}2H_2O$), manganese acetate ($Mn(OAc)_2{\cdot}4H_2O$) and citric acid ($C_6H_8O_7{\cdot}H_2O$) as raw materials, followed by calcination at 500 °C for 12 h in air. The $LiMn_2O_4$ showed a high specific capacity as well as good cyclability in 5 M $LiNO_3$ solution, with 71.3% retention of the initial capacity after 1500 charge/discharge cycles at a high current rate of 1000 mA g^{-1}.

In order to further improve the cyclic stability, in the present work, a series of Al-doped $LiAl_xMn_{2-x}O_4$ materials were synthesized using the above mentioned solid-phase reaction

* Corresponding author. Tel.: +86 21 66134851; fax: +86 21 66132797.
E-mail address: abyuan@shu.edu.cn (A. Yuan).

0378-7753/$ – see front matter © 2010 Elsevier B.V. All rights reserved.
doi:10.1016/j.jpowsour.2010.01.074

method starting with the reactants $LiOAc{\cdot}2H_2O$, $Mn(OAc)_2{\cdot}4H_2O$, $Al(NO_3)_3{\cdot}9H_2O$ and $C_6H_8O_7{\cdot}H_2O$. This study focuses on the effects of calcination temperature and calcination time on the structure of the $LiAl_{0.1}Mn_{1.9}O_4$ materials and their electrochemical performances in 5 M $LiNO_3$ aqueous solution, especially in respect to long-term charge/discharge cyclability at a high current rate in comparison with the pristine $LiMn_2O_4$.

2. Experimental

2.1. Preparation of $LiAl_{0.1}Mn_{1.9}O_4$ materials

Given amount of $LiOAc{\cdot}2H_2O$, $Mn(OAc)_2{\cdot}4H_2O$, $Al(NO_3)_3{\cdot}9H_2O$ and $C_6H_8O_7{\cdot}H_2O$ with a stoichiometric molar ratio of 1.0:1.9:0.1:3.0 were mixed in a mortar, and a given amount (5 wt% of total weight of the mixture) of polyethylene glycol (PEG-200) was added to the mixture. The mixture was ground over at room temperature. In the grinding process, the crystalline water in the starting reactants was released gradually, getting the mixture wet. Ground well for about 1 h, a viscous substance was obtained. The viscous substance was dried at 120 °C for 4 h in a drying box and then ground again to fine powder (precursor). The precursor was calcined in air at different temperatures for different durations (at 400, 500, 600 and 700 °C, respectively, for 12 h; at 800 °C for 3, 6 and 12 h, respectively). After cooled to ambient temperature, the $LiAl_{0.1}Mn_{1.9}O_4$ materials were obtained. In addition, for comparison, the $LiAl_{0.05}Mn_{1.95}O_4$ and $LiAl_{0.15}Mn_{1.85}O_4$ materials calcined at 700 °C for 12 h, and the pristine $LiMn_2O_4$ materials calcined at 700 °C and 800 °C respectively for 12 h, were also prepared using the same method.

2.2. Thermal analysis of precursor and characterization of $LiAl_{0.1}Mn_{1.9}O_4$ materials

Thermogravimetric and differential scanning calorimetric analysis (TG–DSC) of the gel precursor of $LiAl_{0.1}Mn_{1.9}O_4$ was performed on a Netzsch STA-409PG/PC differential scanning calorimeter (Germany) with a sample mass of 11.6 mg. The TG and DSC curves were recorded in a static atmosphere at a heating rate of 10 °C min^{-1} from room temperature to 900 °C. X-ray diffraction analysis of the $LiAl_{0.1}Mn_{1.9}O_4$ materials was conducted on a Rigaku D/max-2000 X-ray powder diffractometer (Japan) with a Cu Kα radiation (40 kV, 200 mA) scanned over the 2θ range of 10–90°. Morphology observation of the $LiAl_{0.1}Mn_{1.9}O_4$ products was carried out using a JEOL JEM-200CX transmission electron microscope (TEM, Japan).

2.3. Preparation and electrochemical testing of $LiAl_{0.1}Mn_{1.9}O_4$ electrodes

The $LiAl_{0.1}Mn_{1.9}O_4$ electrodes were prepared as follows: $LiAl_{0.1}Mn_{1.9}O_4$ active material, acetylene black conductor and polytetrafluoroethylene binder (PTFE emulsion) with the mass ratio of 75:20:5 were mixed completely to form slurry. The slurry was coated onto a titanium mesh current collector with an apparent area of 1 cm × 1 cm, and dried at 80 °C for 12 h and finally roll pressed to ca. 0.6 mm thick. Other test electrodes were prepared with the identical procedure.

Electrochemical tests of the $LiAl_{0.1}Mn_{1.9}O_4$ electrodes and the other test electrodes were performed with a three-electrode cell, in which a $LiAl_{0.1}Mn_{1.9}O_4$ electrode (or other test electrode), an activated carbon electrode, and a saturated calomel electrode (SCE) were served as the working electrode, the counter electrode, and the reference electrode, respectively. Aqueous solution of 5 M $LiNO_3$ was used as the electrolyte. Cyclic voltammetry experiments were carried out using a Solartron 1287 Electrochemical Interface coupled with a 1255B Frequency Response Analyzer (England). Galvanostatic charge/discharge tests were performed using a LAND CT2001A auto-cycler (China). All the work was done at the temperature of 30 °C.

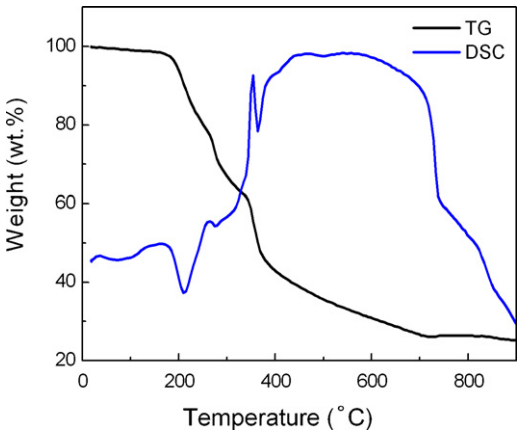

Fig. 1. TG–DSC curves of $LiAl_{0.1}Mn_{1.9}O_4$ precursor.

3. Results and discussion

3.1. TG–DSC analysis of precursor

Fig. 1 shows the TG and DSC curves of the $LiAl_{0.1}Mn_{1.9}O_4$ precursor. The weight loss prior to ca. 180 °C along with an endothermic peak should be attributed to the removal of a small amount of water in the gel precursor. The weight loss in the temperature range of ca. 180–340 °C should be ascribed to the decomposition of organic and inorganic acid radicals in the gel polymeric network. Correspondingly, a strong endothermic peak can be observed around 210 °C in the DSC curve. The quick weight loss in the temperature range of 340–360 °C can be assigned to the oxidative combustion of organic acid radicals along with a corresponding strong and sharp exothermic peak in the DSC curve. In the meanwhile, lithium manganese oxide is formed gradually in this stage. The weight loss from 360 to 700 °C should be the continuous oxidation of residual organic acid radicals along with a wide exothermic peak. As can be seen, no weight loss in the range of ca. 700–800 °C, suggesting that $LiAl_{0.1}Mn_{1.9}O_4$ is thermostable prior to 800 °C. The slow and slight weight loss over 800 °C should be attributed to the decomposition of $LiAl_{0.1}Mn_{1.9}O_4$. The above results suggest that the $LiAl_{0.1}Mn_{1.9}O_4$ would be formed at ca. 340–360 °C and completed at ca. 700 °C. However, the $LiAl_{0.1}Mn_{1.9}O_4$ tends to decompose at ca. 800 °C. Hence, in the present study, the $LiAl_{0.1}Mn_{1.9}O_4$ materials were prepared in the calcination temperature range from 400 °C to 800 °C.

3.2. Structure characterization and morphology observation

Fig. 2(a) shows the XRD patterns of the $LiAl_{0.1}Mn_{1.9}O_4$ materials obtained at different calcination temperatures for 12 h. Fig. 2(b) is the selective enlargement of Fig. 2(a). As can be seen in Fig. 2(a), the diffractions at 2θ = 18.7°, 36.2°, 37.9°, 44.0°, 48.2°, 58.2°, 64.1°, 67.0°, 75.6°, 76.8°, 80.6° and 83.7° are the characteristic diffractions of the cubic spinel $LiMn_2O_4$ with *Fd*3*m* space group (PDF 35-0782). In addition, for the sample obtained at 500 °C calcination, a very weak diffraction at 33.0° can be observed, which corresponds to the strongest characteristic diffraction peak of Mn_2O_3 (PDF 78-0390). This suggests that the material contains trace amount of Mn_2O_3 impurity. In fact, in our previous study [29], the pristine $LiMn_2O_4$ material obtained under the same conditions contains also trace

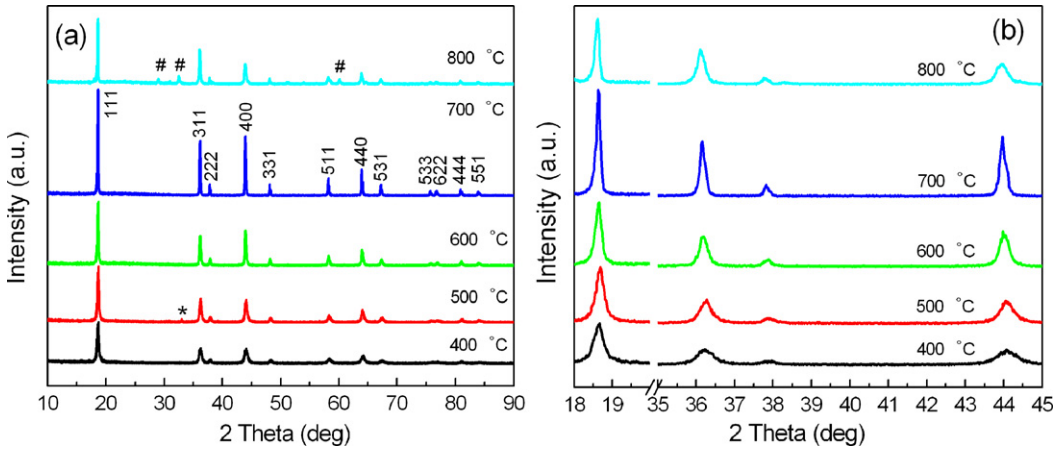

Fig. 2. XRD patterns (a) and their selective enlargements (b) of $LiAl_{0.1}Mn_{1.9}O_4$ materials calcined at different temperatures for 12 h.

amount of Mn_2O_3 impurity. The sample obtained at 800 °C presents three weak diffractions at 29.0°, 32.5° and 60.0°, respectively, corresponding to the several strongest characteristic diffractions of Mn_3O_4 (PDF 80-0382), suggesting the presence of a small amount of Mn_3O_4 impurity. As can be seen, when the calcination temperature is gradually increased from 400 °C to 700 °C, the diffraction intensities of the spinels are also increased, and the diffraction peaks shift to lower angles. These suggest that the crystallinity and grain size of the spinel crystal increase with increasing calcination temperature. However, when the temperature is further increased to 800 °C, the peak intensities are lower than those of the 700 °C derivate. This is because that calcination at the high temperature of 800 °C for a long time will lead to partial decomposition of $LiAl_{0.1}Mn_{1.9}O_4$ to Mn_3O_4, and result in a reduced relative amount of $LiMn_2O_4$ phase in the material. In addition, for the pristine $LiMn_2O_4$, when the calcination temperature is increased from 700 °C to 800 °C, a small amount of Mn_3O_4 impurity phase and the reduced characteristic diffraction intensities can be also observed in the XRD pattern of the 800 °C calcined product (data not shown), which are similar to the Al-doped spinel. Besides, as can be seen in Fig. 2(b), the diffractions of the $LiAl_{0.1}Mn_{1.9}O_4$ shift toward lower 2θ angles gradually when the calcination temperature is increased from 500 to 800 °C, suggesting an increase in lattice constant. Table 1 lists the lattice constants and unit cell volumes of the $LiAl_{0.1}Mn_{1.9}O_4$ materials calcined at different temperatures for 12 h, which are obtained by cell refinement using the XRD data.

Comparing the XRD pattern of the present $LiAl_{0.1}Mn_{1.9}O_4$ calcined at 500 °C with that of the prior pristine $LiMn_2O_4$ obtained under the same conditions [29], we will see that Al-doping shifts the diffractions of $LiMn_2O_4$ toward larger 2θ angles, and correspondingly, the lattice constant a is decreased from 8.2756 to 8.2139 Å. It is well known that $LiMn_2O_4$ takes the face-centered cubic framework of spinel structure with $Fd3m$ space group, in which the Li^+ ions occupy the tetrahedral 8a sites, while the Mn^{3+}, Mn^{4+} (and the doping Al^{3+}) ions reside at the octahedral 16d sites, and the O^{2-} ions are located at the 32e sites. For simplicity, the spinel $LiAl_{0.1}Mn_{1.9}O_4$ can be expressed as $[Li^+]_{8a}[Al^{3+}{}_{0.1}Mn^{3+}{}_{0.9}Mn^{4+}]_{16d}[O^{2-}{}_4]_{32e}$ [3,30]. The radii of Al^{3+}, Mn^{3+} and Mn^{4+} are 0.053, 0.066 and 0.060 nm [31], respectively. Because the radius of Al^{3+} is smaller than that of Mn^{3+}, the partial substitution of Al^{3+} for Mn^{3+} can induce lattice contraction, resulting in a decreased lattice constant, and hence shifts the diffractions toward larger 2θ angles.

Fig. 3(a) shows the XRD patterns of the $LiAl_{0.1}Mn_{1.9}O_4$ materials obtained at the calcination temperature of 800 °C for different durations. Fig. 3(b) is the selective enlargement of Fig. 3(a). As can be seen in Fig. 3(a), no significant difference could be observed between the XRD patterns of the $LiAl_{0.1}Mn_{1.9}O_4$ materials calcined for 3 and 6 h. However, the diffraction intensities of the product calcined for 12 h are obviously lower than those of the 3 and 6 h derivates, due to the presence of Mn_3O_4 phase. In addition, it can be seen from Fig. 3(b) that with increase in calcination time, the characteristic diffractions shift toward smaller 2θ angles, indicating an increase in lattice constant (see Table 2).

TEM photographs of the $LiAl_{0.1}Mn_{1.9}O_4$ materials obtained at different calcination temperatures for different durations are displayed in Fig. 4. It can be seen from Fig. 4(a)–(d) that under the condition of 12 h calcination, the grain size and crystallinity increase with increasing calcination temperature, which is in agreement with the XRD results. Besides, the agglomeration of crystallites becomes more notable, especially for the material calcined at 800 °C for 12 h. As can be seen in Fig. 5(e), the material calcined at 800 °C for a shorter time of 6 h shows a regular crystal form with noticeable edges and corners, and its grain size is obviously larger than that of the material calcined at 700 °C for 12 h.

3.3. Electrochemical performance

Fig. 5 shows the cyclic voltammographs (CVs) of the $LiAl_{0.1}Mn_{1.9}O_4$ electrodes derived from different calcination temperatures for 12 h. The CVs are recorded at a scan rate of 1 mV s^{-1} in 5 M $LiNO_3$ solution, and the current data in A g^{-1} are calculated based on the mass of the $LiAl_{0.1}Mn_{1.9}O_4$ active material. As can be seen, the 800 °C calcined material exhibits two distinct couples of oxidation and reduction, which are similar to that of $LiMn_2O_4$ in nonaqueous electrolytes [32,33]. The abstraction and insertion

Table 1
Lattice constants and cell volumes of $LiAl_{0.1}Mn_{1.9}O_4$ materials calcined at different temperatures for 12 h.

	Temperature (°C)				
	400	500	600	700	800
Lattice constant (a) (Å)	8.2223	8.2139	8.2232	8.2328	8.2357
Cell volume (Å^3)	555.88	554.18	556.05	558.02	558.61

Table 2
Lattice constants and cell volumes of $LiAl_{0.1}Mn_{1.9}O_4$ materials calcined at 800 °C for different durations.

	Calcination time (h)		
	3	6	12
Lattice constant (a) (Å)	8.2187	8.2228	8.2357
Cell volume (Å^3)	555.15	555.98	558.61

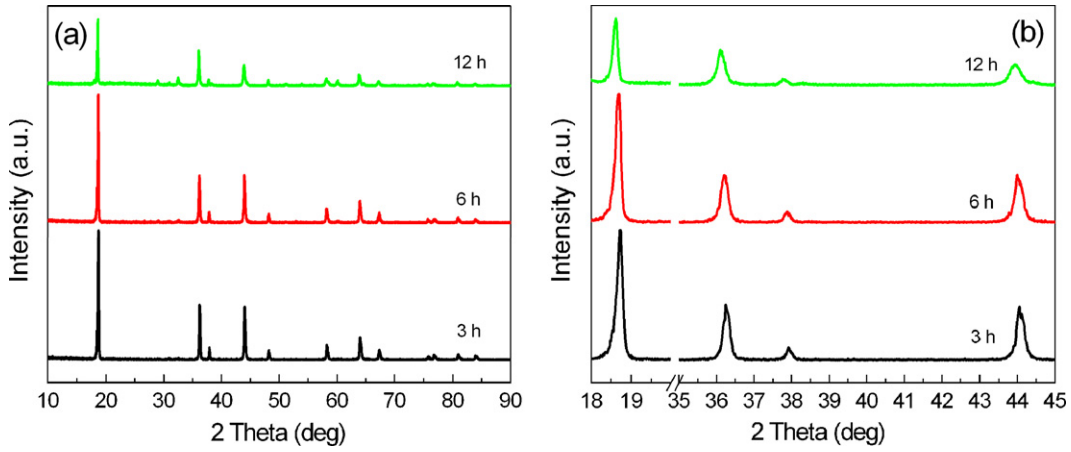

Fig. 3. XRD patterns (a) and their selective enlargements (b) of $LiAl_{0.1}Mn_{1.9}O_4$ materials calcined at 800 °C for different durations.

reaction of the $LiAl_{0.1}Mn_{1.9}O_4$ electrode can be expressed as

$$LiAl_{0.1}Mn_{1.9}O_4 \rightleftharpoons Li_{1-x}Al_{0.1}Mn_{1.9}O_4 + xLi^+ + xe^-$$

the two couples of redox waves should be attributed to Li^+ ions abstraction from and insertion into the two different lattice sites in the spinel [34]. While, the two couples of redox waves for the electrodes derived from lower calcination temperatures seem to be overlapped. The presence of the two distinct couples of redox waves for the 800 °C derived material is likely attributed to the high crystallinity. From 400 °C to 700 °C, the current response increases gradually with increasing temperature, suggesting an increased electrochemical activity (or specific capacity) of the materials obtained at an elevated calcination temperature. This result is similar to the reported electrochemical performances of the Pechini-derived nanocrystalline $LiMn_2O_4$ materials (calcined at different temperatures) in nonaqueous electrolyte [35]. However, when the temperature is further increased from 700 °C to 800 °C, the current response is obviously decreased owing to the Mn_3O_4 formation. Nevertheless, the 800 °C calcined material exhibits excellent cyclic stability (see Fig. 11).

Calcination at 800 °C seems to be of benefit to better cyclic stability, but on the other hand, calcination at this high temperature for a long time will result in lower specific capacity due to the partial decomposition of $LiAl_{0.1}Mn_{1.9}O_4$. In order to obtain a $LiAl_{0.1}Mn_{1.9}O_4$ material with high specific capacity as well as good cyclic stability, two materials calcined at 800 °C for a shorter time of 3 and 6 h, respectively, were also prepared and electrochemically tested. As can be seen in Fig. 6, the CVs of the materials calcined at 800 °C for different durations are different. The two couples of redox waves become more distinguishable gradually as the calcination time is increased. This suggests that longer calcination is in favor of obtaining a material with higher crystallinity. However, the current of the electrode derived from 12 h calcination is much lower than that of the 3 and 6 h derivates. From the XRD, TEM and CV results, it follows that calcination at 800 °C for 6 h is of benefit to obtaining a $LiAl_{0.1}Mn_{1.9}O_4$ material with high crystallinity and high specific capacity.

Fig. 7 shows the current–rate dependence of discharge specific capacities of the $LiAl_{0.1}Mn_{1.9}O_4$ electrodes derived from different calcination temperatures for 12 h. The electrodes are charge/discharge cycled in the operating potential range of 0.2–1.3 V (SCE) at various current rates of 500, 600, 700, 800, 900 and 1000 mA g^{-1}, respectively. As can be seen, the specific capacities of the electrodes at any a current rate follow the order of 700 °C > 600 °C > 500 °C > 400 °C > 800 °C. This is consistent with the CV results in Fig. 5. However, the rate capability of the electrode derived from the higher calcination temperature of 700 °C or 800 °C is a little poor than that of the others. This may be ascribed to their larger grain sizes. Nevertheless, in general, all the electrodes exhibit good rate capability. For example, from 500 to 1000 mA g^{-1}, the specific capacity of the 700 °C derived electrode is decreased from 122.3 to 108.1 mAh g^{-1}, i.e., decreased only by 11.6%.

Fig. 8 shows the rate capabilities of the $LiAl_{0.1}Mn_{1.9}O_4$ electrodes derived from calcination at 800 °C for different durations. As can be seen, the specific capacities of the electrodes follow the order of 3 h > 6 h > 12 h. The corresponding charge/discharge curves at the current rate of 500 mA g^{-1} are shown in Fig. 9, where two charge/discharge plateaus could be observed, corresponding to the two redox waves in the CV curves. In addition, the two plateaus become more distinguishable with increasing calcination time, which is in agreement with the CV results in Fig. 6.

Fig. 10 shows the cycle performances of the $LiAl_{0.1}Mn_{1.9}O_4$ electrodes derived from different calcination temperatures for 12 h. The electrodes are charge/discharge cycled at the high current rate of 1000 mA g^{-1} over the potential range of 0.2–1.3 V (SCE). As can be seen, the initial specific capacities of the electrodes increase with increasing calcination temperature, and the 600 °C and 700 °C derivates show obviously higher initial specific capacities than the 400 °C and 500 °C derivates. Besides, the cyclic stability increases gradually with increase in calcination temperature. About 70% of initial capacity is retained after 1100, 1800, 2700 and 4600 cycles for the materials calcined at 400 °C, 500 °C, 600 °C and 700 °C, respectively. In addition, it is worthy to note that the initial specific capacity of the $LiAl_{0.1}Mn_{1.9}O_4$ calcined at 500 °C in the present study is a little lower than that of the pristine $LiMn_2O_4$ prepared under the same conditions in our prior work [29], but the cyclic stability of the Al-doped $LiAl_{0.1}Mn_{1.9}O_4$ is superior to that of the pristine $LiMn_2O_4$. Theoretically, the capacity of a doped $LiMn_2O_4$ is in proportion to the concentration of Mn^{3+} in the spinel [30]. Hence, a partial substitution of Al^{3+} for Mn^{3+} will result in a decreased capacity. The improved cyclic stability of the Al-doped spinel should be attributed mainly to the suppression of Jahn–Teller distortion of the cubic spinel with a decreased Mn^{3+} in the structure.

The cycle performances of the $LiAl_{0.1}Mn_{1.9}O_4$ electrodes derived from calcination at 800 °C for different durations are shown in Fig. 11. For comparison, the cycle performance of the pristine $LiMn_2O_4$ calcined at 800 °C is also placed in Fig. 11. As can be seen, the initial specific capacities of the $LiAl_{0.1}Mn_{1.9}O_4$ electrodes decrease with increasing calcination time. Although the electrode derived from 3 h calcination shows a higher initial specific capacity, its cyclic stability is poor. Whereas, the electrode derived from 6 and 12 h calcination, respectively, exhibit far prolonged cyclic stability, especially for the 12 h derivate. After 1600, 5300 and 8000

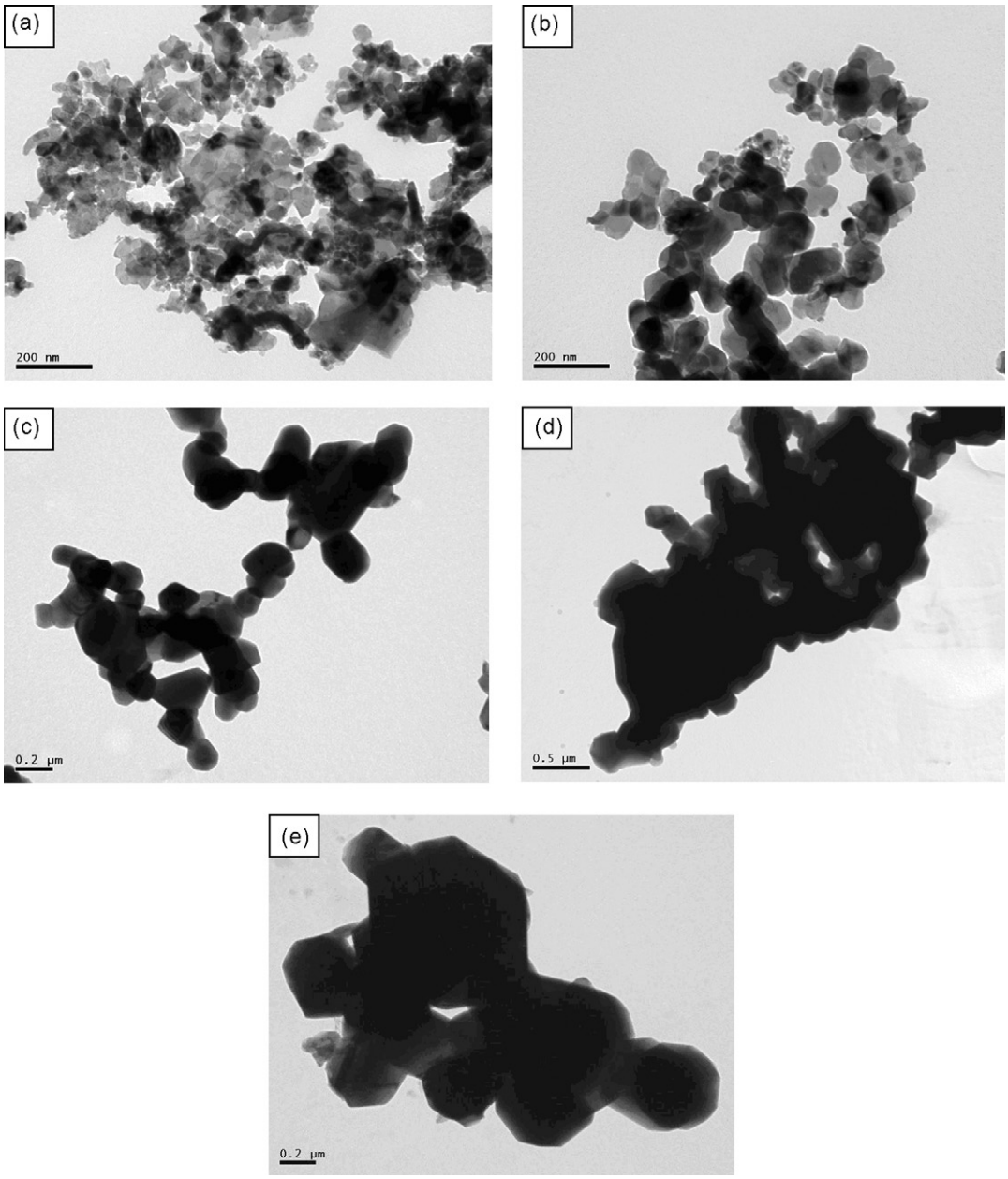

Fig. 4. TEM photographs of $LiAl_{0.1}Mn_{1.9}O_4$ materials calcined at different temperatures for different durations. (a) 500 °C, 12 h; (b) 600 °C, 12 h; (c) 700 °C, 12 h; (d) 800 °C, 12 h; (e) 800 °C, 6 h.

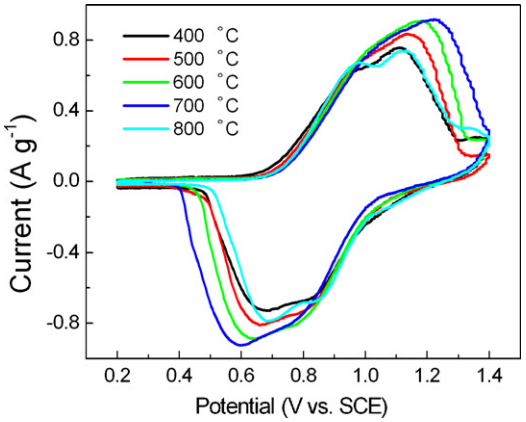

Fig. 5. CVs of $LiAl_{0.1}Mn_{1.9}O_4$ electrodes derived from calcination at different temperatures for 12 h.

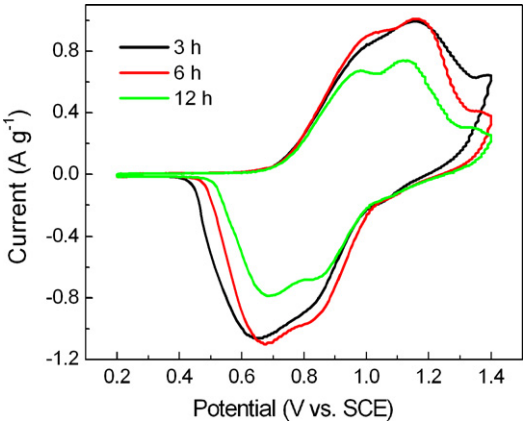

Fig. 6. CVs of $LiAl_{0.1}Mn_{1.9}O_4$ electrodes derived from calcination at 800 °C for different durations.

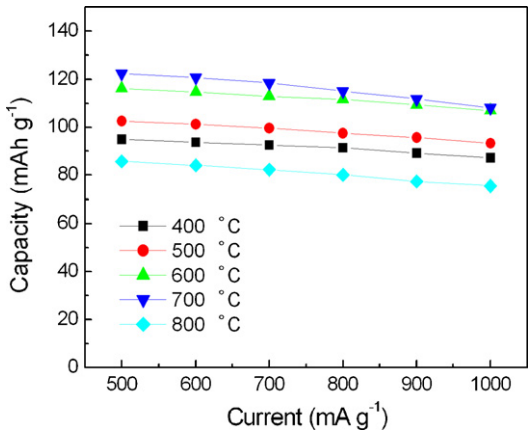

Fig. 7. Rate capabilities of $LiAl_{0.1}Mn_{1.9}O_4$ electrodes derived from different calcination temperatures for 12 h.

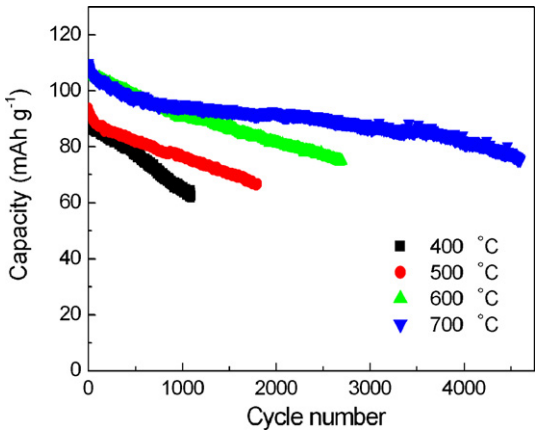

Fig. 10. Cycle performances of $LiAl_{0.1}Mn_{1.9}O_4$ electrodes derived from different calcination temperatures for 12 h at a current rate of 1000 mA g^{-1}.

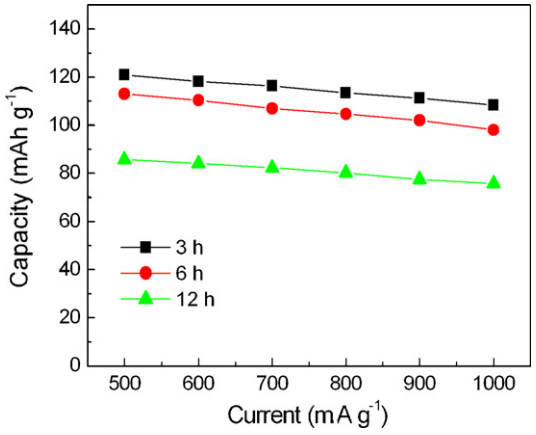

Fig. 8. Rate capabilities of $LiAl_{0.1}Mn_{1.9}O_4$ electrodes derived from calcination at 800 °C for different durations.

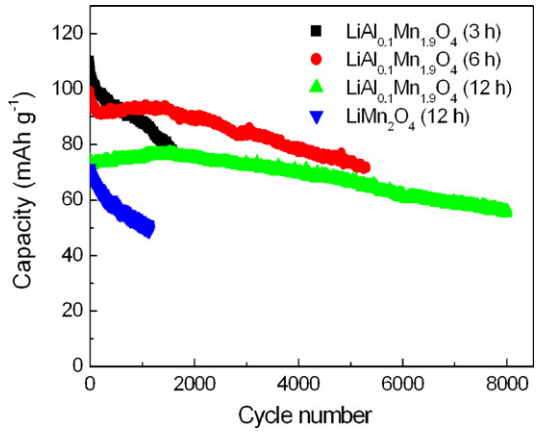

Fig. 11. Cycle performances of $LiAl_{0.1}Mn_{1.9}O_4$ and $LiMn_2O_4$ electrodes derived from calcination at 800 °C for different durations at a current rate of 1000 mA g^{-1}.

charge/discharge cycles, capacity retentions of 70.0%, 72.2% and 75.6% are achieved for the electrodes derived from 3, 6 and 12 h calcination, respectively. It is evident that the cyclic stability of the material calcined for 12 h is superior to that of the material calcined for 6 h, but the specific capacity of the former is lower than that of the latter due to the presence of Mn_3O_4 impurity. The increased cyclic stability with increasing calcination temperature and calcination time may be attributed to the higher crystallinity and larger crystal size of the material calcined at an elevated temperature for a prolonged time. Compared with the pristine $LiMn_2O_4$ calcined at 800 °C for 12 h, the cyclic stability of the $LiAl_{0.1}Mn_{1.9}O_4$ calcined at 800 °C for 12 h is much improved. This further confirms the positive effect of Al-doping on the cyclability.

Fig. 12 shows the cycle performances of the $LiAl_xMn_{2-x}O_4$ calcined at 700 °C for 12 h. Compared with the pristine $LiMn_2O_4$, Al-doping can remarkably improve the cyclability, and the

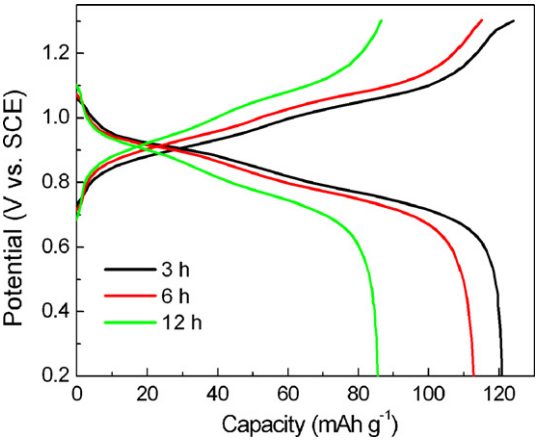

Fig. 9. Charge/discharge curves of $LiAl_{0.1}Mn_{1.9}O_4$ electrodes derived from calcination at 800 °C for different durations at a current rate of 500 mA g^{-1}.

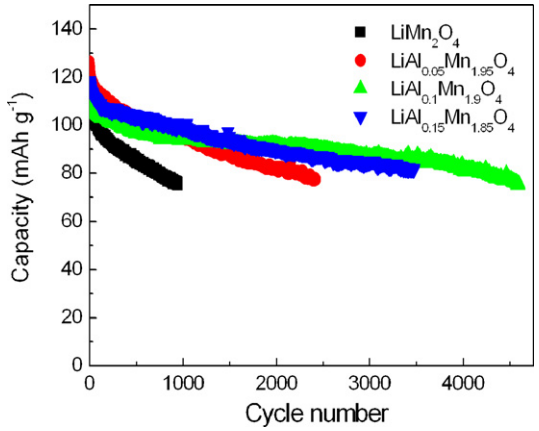

Fig. 12. Cycle performances of $LiAl_xMn_{2-x}O_4$ electrodes derived from calcination at 700 °C for 12 h at a current rate of 1000 mA g^{-1}.

$LiAl_{0.1}Mn_{1.9}O_4$ exhibits the best cyclability. From the above experimental results, we will arrive at a conclusion that an appropriate amount of Al doping is the essential reason for stabilization of the spinel upon cycling. In addition, high crystallinity of the spinel, which can be achieved by calcination at a higher temperature for sufficient time, would also play an important role in acquisition of the good cyclability.

4. Conclusions

In this paper, spinel $LiAl_xMn_{2-x}O_4$ materials were prepared by room-temperature solid-phase grinding reaction followed by calcination at different temperatures for different durations. XRD results revealed that the crystallinity of the $LiAl_{0.1}Mn_{1.9}O_4$ increases with increasing calcination temperature and calcination time. At an elevated calcination temperature of 800 °C, a small amount of Mn_3O_4 impurity can be detected when calcined for 12 h, owing to the decomposition of $LiAl_{0.1}Mn_{1.9}O_4$, but no evidence of impurity phase can be observed when calcined for a shorter time of 3 or 6 h. TEM results demonstrated that the grain size of the prepared materials increase with increasing calcination temperature. Electrochemical experiments showed that the cyclability of the $LiAl_{0.1}Mn_{1.9}O_4$ materials increase with increase in calcination temperature and calcination time. An appropriate amount of Al doping can significantly improve the cyclability of the $LiMn_2O_4$ spinel in an aqueous media. Besides, high crystallinity of the spinel is also important to good cyclability. Al-doped $LiMn_2O_4$ is a promising candidate positive electrode material for aqueous energy storage devices, such as aqueous lithium ion batteries or supercapacitors.

Acknowledgements

This work was supported by Leading Academic Discipline Project of Shanghai Municipal Education Commission (Project Number: J50102). Center of Instrumental Analysis and Test of Shanghai University is gratefully acknowledged for XRD and TEM experiments.

References

[1] V.G. Kumar, J.S. Gnanaraj, S. Ben-David, D.M. Pickup, E.R.H. van-Eck, A. Gedanken, D. Aurbach, Chem. Mater. 15 (2003) 4211.
[2] J.Y. Luo, Y.G. Wang, H.M. Xiong, Y.Y. Xia, Chem. Mater. 19 (2007) 4791.
[3] W.J. Zhou, S.J. Bao, B.L. He, Y.Y. Liang, H.L. Li, Electrochim. Acta 51 (2006) 4701.
[4] L.F. Xiao, Y.Q. Zhao, Y.Y. Yang, Y.L. Cao, X.P. Ai, H.X. Yang, Electrochim. Acta 54 (2008) 545.
[5] W. Cho, W. Ra, J. Shirakawa, M. Nakayama, M.J. Wakihara, Solid State Chem. 179 (2006) 3534.
[6] D. Zhang, B.N. Popov, R.E. White, J. Power Sources 76 (1998) 81.
[7] R. Thirunakaran, K.T. Kim, Y.M. Kang, C.Y. Seo, J. Young-Lee, J. Power Sources 137 (2004) 100.
[8] K. Suryakala, G.P. Kalaignan, T. Vasudevan, Mater. Chem. Phys. 104 (2007) 479.
[9] Y.S. Lee, Y.K. Sun, S. Ota, T. Miyashita, M. Yoshio, Electrochem. Commun. 4 (2002) 989.
[10] Y. Idemoto, H. Sekine, K. Ui, N. Koura, Solid State Ionics 176 (2005) 299.
[11] S. Patoux, L. Sannier, H. Lignier, Y. Reynier, C. Bourbon, S. Jouanneau, F.L. Cras, S. Martinet, Electrochim. Acta 53 (2008) 4137.
[12] R. Vidu, P. Stroeve, Ind. Eng. Chem. Res. 43 (2004) 3314.
[13] A.R. Han, T.W. Kim, D.H. Park, S.J. Hwang, J.H.J. Choy, Phys. Chem. C 111 (2007) 11347.
[14] J. Tu, X.B. Zhao, J. Xie, G.S. Cao, D.G. Zhuang, T.J. Zhu, J.P.J. Tu, Alloys Compd. 432 (2007) 313.
[15] R. Singhala, M.S. Tomar, J.G. Burgos, R.S. Katiyara, J. Power Sources 183 (2008) 334.
[16] W. Li, J.R. Dahn, D.S. Wainwright, Science 264 (1994) 1115.
[17] W. Li, J.R.J. Dahn, Electrochem. Soc. 142 (1995) 1742.
[18] N.C. Li, C.J. Patrissi, G.L. Che, C.R.J. Martin, Electrochem. Soc. 147 (2000) 2044.
[19] A. Eftekhari, Electrochim. Acta 47 (2001) 495.
[20] B.J. Hwang, Y.W. Tsai, R. Santhanam, S.K. Hu, H.S. Sheu, J. Power Sources 119–121 (2003) 727.
[21] M. Jayalakshmi, M.M. Rao, F. Scholz, Langmuir 19 (2003) 8403.
[22] J.W. Lee, S.I. Pyun, Electrochim. Acta 49 (2004) 753.
[23] N. Nakayama, T. Nozawa, Y. Iriyama, T. Abe, Z. Ogumi, K. Kikuchi, J. Power Sources 174 (2007) 695.
[24] N. Cvjeticanin, I. Stojkovic, M. Mitric, S. Mentus, J. Power Sources 174 (2007) 1117.
[25] D. Tonti, M.J. Torralvo, E. Enciso, I. Sobrados, J. Sanz, Chem. Mater. 20 (2008) 4783.
[26] P. He, J.Y. Luo, J.X. He, Y.Y. Xia, J. Electrochem. Soc. 156 (2009) A209.
[27] K. Katakura, K. Wada, Y. Kajiki, A. Yamamoto, Z. Ogumi, J. Power Sources 189 (2009) 240.
[28] N. Nakayama, I. Yamada, Y. Huang, T. Nozawa, Y. Iriyama, T. Abe, Z. Ogumi, Electrochim. Acta 54 (2009) 3428.
[29] L. Tian, A.B. Yuan, J. Power Sources 192 (2009) 693.
[30] T. Kakuda, K. Uematsu, K. Toda, M. Sato, J. Power Sources 167 (2007) 499.
[31] T.F. Yi, X.G. Hu, K. Gao, J. Power Sources 162 (2006) 636.
[32] C.H. Jiang, S.X. Dou, H.K. Liu, M. Ichihara, H.S. Zhou, J. Power Sources 172 (2007) 410.
[33] T. Doi, T. Yahiro, S. Okada, Yamaki, J. Electrochim. Acta 53 (2008) 8064.
[34] N.N. Sinha, P. Ragupathy, H.N. Vasan, N. Munichandraiah, Int. J. Electrochem. Sci. 3 (2008) 691.
[35] S. Vivekanandhan, M. Venkateswarlu, N. Satyanarayana, P. Suresh, D.H. Nagaraju, N. Munichandraiah, Mater. Lett. 60 (2006) 3212.